Hydrazine method of synthesis of γ-Fe_2O_3 useful in ferrites preparation. Part IV – preparation and characterization of magnesium ferrite, $MgFe_2O_4$ from γ-Fe_2O_3 obtained from hydrazinated iron oxyhydroxides and iron (II) carboxylato-hydrazinates

K. S. RANE*, V. M. S. VERENKAR, P. Y. SAWANT
Department of Chemistry, Goa University, Goa 403206, India
E-mail: ksrane@unigoa.ernet.in

Electro-magnetic properties and microstructural characterization of $MgFe_2O_4$ synthesized by a ceramic technique at $\sim$ 1000 °C from iron oxides, consisting of mainly γ-Fe_2O_3 and traces of α-Fe_2O_3, prepared from iron ore rejects, are compared with the ferrite obtained from commercial α-Fe_2O_3. The sources of γ-Fe_2O_3 are hydrazinated iron (II) carboxylates and iron oxyhydroxides which autocatalytically decompose giving mainly γ-Fe_2O_3 of uniform particles of 10–30 nm (by scanning electron microscopy (SEM) studies) having high surface area. The ferrite synthesized from such nanoparticle size γ-Fe_2O_3 gave a porosity of $\sim$ 25% with grains ranging from 0–3 μm. On the other hand, $MgFe_2O_4$ obtained from commercial α-Fe_2O_3 grains (of 1–2 μm size) gave particles of 0–6 μm with a porosity $\sim$ 42%. Saturation magnetization values 922–1168 G are found for $MgFe_2O_4$ from γ-Fe_2O_3 source while the α-Fe_2O_3 source gave the lowest value, $\sim$ 609. The Curie temperature, T_c, from magnetic susceptibility, initial permeability and resistivity measurements indicated a highest T_c of $\sim$ 737 K for $MgFe_2O_4$ from α-Fe_2O_3, while lower values are found for the ferrite prepared from γ-Fe_2O_3.

1. Introduction

Alpha iron oxide, α-Fe_2O_3 (hematite) is the major raw material amounting to more than 70% in the raw meal in the synthesis of ferrites (soft and hard). The other metals that are required for completing the desired ferrite are taken in the form of oxides, MO, or easily decomposable metal carbonates, hydroxides or nitrates. A homogeneous mixing of these raw materials needs a thorough grinding to uniform size. To initiate the solid state reactions a well programmed heat treatment with intermittent grinding and pelletizing is needed to finally produce a suitable sintering process at higher temperatures to achieve a single phase ferrite in the ceramic technique, However, there are a few reports in the literature that suggest the use of γ-Fe_2O_3 instead of α-Fe_2O_3 in ferrite synthesis. In one such study iron oxide consisting of a larger portion of gamma ferric oxide, γ-Fe_2O_3 (maghemite, spinel) is used [1] in the synthesis of ferrites, zinc and barium ferrite and it was found that the reaction rate between Fe_2O_3 and MO increases and the ferrites are formed at a much lower temperature than using the normal α-Fe_2O_3. In nickel–zinc ferrite preparation it has been noticed [2] that the magnetic performance parameters and resistivity values show that γ-Fe_2O_3 is a better precursor than α-Fe_2O_3.

In barium ferrite synthesis, natural magnetite, Fe_3O_4 (inverse spinel) is found to give better electromagnetic characteristics and large reserves of natural magnetites are, thus, used successfully for producing ferrite magnets in Vietnam [3]. The magnetite has a phase transition from Fe_3O_4 to Fe_2O_3 in the heating process and due to the high reactivity of the phase transformation, the ferritization occurs readily and is completed more rapidly using the iron oxide, Fe_2O_3.

Magnetite, as spinel iron sand found on the west coast of the North island of New Zealand, was used [4] in the synthesis of nickel ferrites and their properties compared with the ferrite prepared from hematite (α-Fe_2O_3) and pure synthetic magnetite (Fe_3O_4). All three starting materials form $NiFe_2O_4$ in air. The reaction in magnetite proceeds via an oxidation step at 220 °C. Inert atmospheres are also used in the synthesis of the ferrite and from Mössbauer studies the cation distributions are determined. The magnetic saturation moment of the ferrite derived from iron sand, both in air and nitrogen, is smaller than that obtained from pure iron oxides, as Ti^{+4} present in iron sand appeared on the octahedral sites of the ferrite.

In the hydrothermal method, barium hexaferrite has

0957–4522

been synthesized [5, 6] from γ-Fe_2O_{3s} and $Ba(OH)_2$ in an alkaline solution at high temperatures and pressures in a closed batch reactor.

We are studying this aspect of using iron oxides (mainly γ-Fe_2O_3) in synthesizing $MnZnFe_2O_4$ and $MgFe_2O_4$. The present paper deals with preliminary results on such studies carried out in the preparation of magnesium ferrite, $MgFe_2O_4$. The γ-Fe_2O_3 samples used here are as prepared in part I [7] and part II [8]. Here, we are reporting our investigations carried out on micro-structural aspects of the iron oxides and $MgFe_2O_4$ prepared, from these iron oxides and an attempt has been made to correlate some electro-magnetic characteristics of these ferrites with the ferrite synthesized using commercial grade α-Fe_2O_3 (hematite).

$MgFe_2O_4$ is usually synthesized by routine solid state techniques [9–13] at high temperatures ($> 1100\,^{\circ}C$). Alternative methods for obtaining high quality materials use precursor techniques [14–16]. It has been observed that [12] microstructural characteristics of Mg-Fe spinel powders are affected by the preparative methods and parameters. High reactivity leading to a spinel with a uniform particle distribution is possible if the starting materials have submicrometer particles.

This study is significant in the sense that the γ-Fe_2O_3 samples that are used here are prepared from iron ore rejects. The detailed chemical beneficiation and preparation are described elsewhere [17]. We have the objective in our current research activities to make use of low grade iron ore rejects in the synthesis of γ-Fe_2O_3 by the hydrazine method to use in ferrite synthesis of technological importance.

2. Experimental

2.1. Preparation of γ-Fe_2O_3

γ-Fe_2O_3 is prepared using various precursors as mentioned in parts I and II [7, 8]. The γ-Fe_2O_3 samples used in the present studies are autocatalytically decomposed end products of

I. Iron (II) carboxylato-hydrazinates:
a) Ferrous fumarato-hydrazinate (FFHA)
b) Ferrous succinato-hydrazinate (FSHA)
c) Ferrous malonato-hydrazinate (FMHA)
d) Ferrous tartrato-hydrazinate (FTHA)

II. Hydrazinated iron (III) oxyhydroxides
a) Hydrazinated γ-FeOOH (γFA)
b) Hydrazinated amorphous FeOOH (AmpFA)
c) Hydrazinated α-FeOOH (αFA)

2.2. Preparation of $MgFe_2O_4$: ceramic technique

2.2.1. γ-Fe_2O_3 + $MgCO_3$

A requisite amount of pure $MgCO_3$ and γ-Fe_2O_3 (described in Section 2.1) were mixed, pelletized and preheated $\sim 800\,^{\circ}C/12\,h$ in air and cooled. After grinding and pelletizing the samples were finally sintered at $1000\,^{\circ}C$ for 24 h in air. The samples prepared were coded as below, depending upon their iron oxide source.

Iron oxide source	code name of magnesium ferrite
(1) FFHA	→ MgFFHA
(2) FSHA	→ MgFSHA
(3) FMHA	→ MgFMHA
(4) FTHA	→ MgFTHA
(5) γFA	→ MgγFA
(6) AmpFA	→ MgAmpFA
(7) αFA	→ MgαFA

2.2.2. Commercial α-Fe_2O_3 + $MgCO_3$

For the comparison of the ferrites prepared from the above γ-Fe_2O_3 samples, a commercial grade hematite, α-Fe_2O_3 (Baker Analysed, 99.9%), was used for $MgFe_2O_4$ preparation as in Section 2.2.1. It is coded as MgHEM.

2.3. Characterization

2.3.1. X-ray characterization

X-ray diffraction measurements of magnesium ferrite samples were carried out on a Rigaku D Max II X-ray diffractometer. The observed *d* values were compared with JCPDS files [18].

2.3.2. Micro-structural characterization

SEM of iron oxides and $MgFe_2O_4$ were taken on a Cambridge Stereoscan S 250 MK III.

2.3.3. Magnetic characterization

2.3.3.1. Saturation magnetization. Saturation magnetization values of the $MgFe_2O_4$ samples were measured on a high field hysteresis loop tracer, described by Likhite *et al.* [19].

2.3.3.2. a.c. Susceptibility. The domain structure and the Curie temperature were determined by the a.c. susceptibility method, developed by Likhite and Radhakrishnamurthy [20].

2.3.3.3. Initial permeability. The initial permeability as a function of temperature was measured at 1 kHz over the temperature range of 300 K to 800 K using a MIC 4060-D LCR meter.

2.3.4. Electrical characterization

2.3.4.1. Resistivity. Direct current (d.c.) electrical resistivity measurements of the $MgFe_2O_4$ samples were carried out from room temperature to $700\,^{\circ}C$ by the usual two probe method.

3. Results and discussion

3.1. X-ray analysis

3.1.1. Thermal products of autocatalytically decomposed iron (II) carboxylato-hydrazinates

The autocatalytically decomposed end products of iron (II) carboxylato-hydrazinates: ferrous fumarato-hydrazinate (FFHA), ferrous succinato-hydrazinate (FSHA),

ferrous malonate-hydrazinate (FMHA) and ferrous tartrato-hydrazinate are magnetic in nature and their X-ray diffraction (XRD) patterns match with the pattern of standard gamma ferric oxide, γ-Fe_2O_3 and the d_{hkl} values of these compare well with the values of JCPDS files [21, 22] for γ-Fe_2O_3. An extra peak at $d = 0.27$ nm is found in these as prepared end products which corresponds to the strongest line of α-Fe_2O_3. The XRD patterns of these are shown in Fig. 1 and, for comparison, the pattern of standard γ-Fe_2O_3 is included. The traces of α-Fe_2O_3 that are found due to the intense heating taking place during autocatalytic decomposition, converting a few particles of γ-Fe_2O_3 to α-Fe_2O_3 magnetic studies carried out [7, 17] on these also show the presence of α-Fe_2O_3.

3.1.2. Thermal products of autocatalytically decomposed hydrazinated iron oxyhydroxides

The autocatalytically decomposed end products of hydrazinated iron oxyhydroxides: γ-FeOOH (γFA), α-FeOOH (αFA) and amorphous FeOOH (AmpFA) are magnetic in nature and their XRD patterns match with the γ-Fe_2O_3, although a few traces of α-Fe_2O_3 are also observed. However, the autocatalytically decomposed hydrazinated γ-FeOOH shows no traces of α-Fe_2O_3 and the γ-Fe_2O_3 obtained thus, is the best of the end products studied here. Magnetic studies above reveal that it has $\sim 71.6\,\mathrm{emul/g}^{-1}$ [8, 17] which is very close to the expected saturation magnetization value for γ-Fe_2O_3 [23]. In Table I, the XRD data are compiled along with the reported d values of different iron oxides.

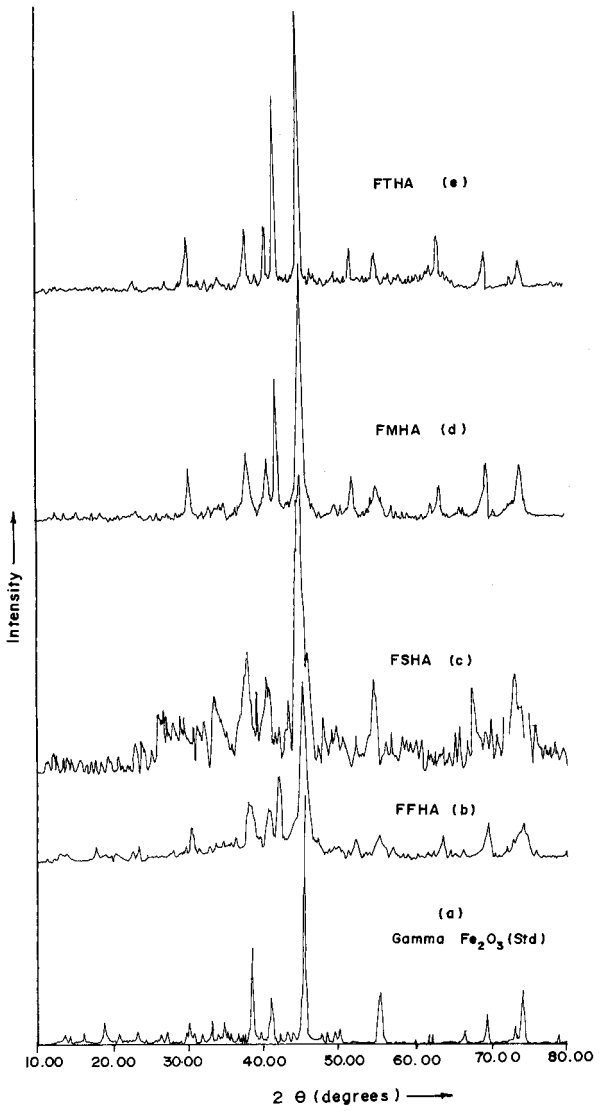

Figure 1 XRD pattern of decomposed end products of iron (II) carboxylato-hydrazinates and standard γ-Fe_2O_3.

3.1.3. Formation of $MgFe_2O_4$

The X-ray diffraction method is used to confirm the formation of magnesium ferrite from iron oxides (mainly γ-Fe_2O_3) that are obtained from various precursors as mentioned in Section 2.1. The XRD patterns of $MgFe_2O_4$ obtained from different iron oxide sources are presented in Fig. 2. For comparison, the XRD pattern of the $MgFe_2O_4$ (MgHEM) obtained from α-Fe_2O_3 is also shown in the figure. Since the patterns of $MgFe_2O_4$ from different iron oxide sources are almost identical, only a representative sample pattern MgFMHA, is shown in the figure.

The calculated d values, considering the cubic structure for the ferrite, agree with the observed d values, as well as with the reported ones for $MgFe_2O_4$ [18] which confirms the single phase spinel formation. The sample MgHEM prepared from commercial α-Fe_2O_3, however, shows some extra peaks and these match with α-Fe_2O_3 suggesting that single phase $MgFe_2O_4$ is not achieved at a temperature of 1000 °C. The lattice parameters of all the magnesium ferrite samples are given in Table II. They are found to be 0.839–0.841 nm which are within the range of the reported values [16, 24–28].

The X-ray densities, dx, of all the samples found in the range 4.45 to 4.49 g cm^{-3} are close to the reported value of 4.52 [29] and the actual density, da, measured enabled us to calculate porosity using the formula,

$$P(\%) = \frac{dx - da}{dx} \times 100$$

All the ferrite samples prepared from γ-Fe_2O_3 (mainly) show porosity of $\sim 25\%$ (Table II), whereas, the spinel synthesized from α-Fe_2O_3 (MgHEM) indicates a high porosity of $\sim 42\%$. Porosities of 31% [30] and 27% [31] were found for $MgFe_2O_4$ obtained at 1100 °C.

The literature survey reveals that the sintering temperature used by researchers for the preparation of $MgFe_2O_4$ by the ceramic method, is 1100 °C and above [12, 26, 30, 32, 33]. In the present study, the sintering temperature of 1000 °C was used for the preparation of impurity-free $MgFe_2O_4$ samples. This was possible as the raw material, iron-oxide, used here was mainly γ-Fe_2O_3 with or without traces of α-Fe_2O_3, which was found to increase the rate of ferritization at lower temperatures [1, 2]. However, the $MgFe_2O_4$ sample prepared from commercial α-Fe_2O_3 (MgHEM) shows an impurity peak of α-Fe_2O_3, suggesting that the sintering temperature is not sufficient to form single phase $MgFe_2O_4$.

TABLE I *d*-values of different iron oxide samples

Sample	*d* values										
γ-Fe_2O_3*	—	2.95	—	—	2.51	2.09	—	1.70	1.60	1.47	1.2
γ-Fe_2O_3*	—	2.95	2.78	—	2.52	2.08	—	1.70	1.61	1.48	1.27
Fe_3O_4*	—	2.97	—	—	2.53	2.09	—	1.71	1.61	1.48	1.28
α-Fe_2O_3*	3.66	—	—	2.70	2.51	2.20	1.83	1.69	—	1.45	—
FFHA	3.68	—	2.78	2.70	2.52	2.08	1.84	1.70	1.60	—	—
FSHA	—	2.95	2.78	—	2.51	2.09	—	1.71	1.61	—	—
FMHA	—	2.97	2.78	2.70	2.52	2.09	1.83	1.70	1.61	—	—
FTHA	—	2.95	2.78	2.70	2.52	2.09	1.84	1.70	1.61	—	—
γFA	—	2.96	—	—	2.52	2.09	—	1.70	1.61	1.48	1.27
AmpFA	—	2.95	—	—	2.51	2.08	—	—	1.60	1.47	1.27
αFA	—	—	—	2.70	2.52	—	1.83	1.69	1.60	1.48	1.27

*Reported

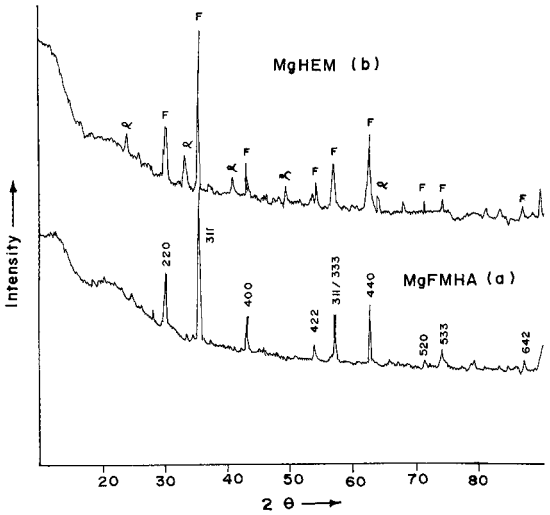

Figure 2 XRD pattern of $MgFe_2O_4$: (a) representative sample from γ-Fe_2O_3 source; (b) from commercial α-Fe_2O_3 (F = ferrite; α = α-Fe_2O_3).

3.2. Magnetic and electrical characterization

3.2.1. Saturation magnetization

Saturation magnetization, σ emu g^{-1} values of all the $MgFe_2O_4$ samples fall in the range 22–28 emu g^{-1} (Table II) except for the ferrite prepared from commercial α-Fe_2O_3 (MgHEM) which shows 17.2 emu g^{-1}. The saturation magnetization values, $4\pi M_s$ in G are also found to be in the range of 922–1168 except for MgHEM which shows the lowest value of 609.5 G (Table II). The magnetone number (n_B) calculated (Table II) shows the lowest value of 0.62 for MgHEM, while the other samples are in the range 0.79–1.01, which are close to the reported values of 0.93–1.2 [9, 34].

3.2.2. a.c. susceptibility

The $\chi - T$ curves indicate multidomain (MD) grains for MgFTHA and predominantly single domain (SD) for the other samples. A sharp fall in the curves at Curie temperature for all samples indicates no impurity phase in the ferrites. The Curie temperatures for the ferrites in the present investigation fall in the range 642–700 K, while the spinel from commercial α-Fe_2O_3 shows the highest T_c of 730 K (Table II). The reported values show a wide range of T_c of 593–713 K [35].

3.2.3. Initial permeability

A sharp decrease in μ_i at the Curie temperature after the initial increase from room temperature suggests a single phase ferrite formation in the present investigations, except for MgHEM. The Curie temperatures, T_c, obtained from such studies are given in Table II. The T_c obtained by this method shows higher values than that observed from magnetic susceptibility measurements.

In general, the $MgFe_2O_4$ samples in the present investigations show lower values of saturation magnetization $(4\pi M_s)$ and magnetone number than the reported one. This is due to the lower temperature (1000 °C) and comparatively shorter duration (24 h) used for sintering which results in higher porosity, thus, decreasing magnetic properties.

TABLE II Lattice parameter, porosity, magnetization data and Curie temperature of magnesium ferrite samples

	Lattice parameter "*a*"	Porosity *P*(%)	Magnetization data				Curie temperature (K)	
Sample			$4\pi Ms_s$ (G)	n_B	σ_s (emu g^{-1})	Magnetic susceptibility	Initial permeability	Resistivity
MgFFHA	8.3927	26.04	1082	0.93	25.96	658	689	672
MgFSHA	8.3912	29.58	967.2	0.87	24.36	670	—	672
MgFMHA	8.3877	26.24	922.3	0.79	22.15	642	667	658
MgFTHA	8.3999	21.31	1097	0.89	24.79	660	682	685
Mg αFA	8.4103	23.63	1110.2	0.93	25.96	700	725	712
Mg γFA	8.4147	26.41	1042.6	0.91	25.34	680	712	699
MgAmpFA	8.4143	25.92	1168.4	1.01	28.2	680	717	698
MgHEM	8.4172	42.19	609.5	0.62	17.2	730	742	739

Grain size and porosity are the important factors which influence magnetic and electrical properties in ceramics. In all samples, except the one synthesized from α-Fe_2O_3, many of the above magnetic characteristics show uniform behavior. X-ray characterization also reveals single phase $MgFe_2O_4$ formation in all samples except the one obtained from α-Fe_2O_3. These results, therefore, suggest that the microstructure of all the samples, except MgHEM, should be similar compared to the one synthesized from α-Fe_2O_3. Therefore, detailed microstructural studies were carried out.

3.2.4. Electrical resistivity

Direct current electrical resistivity measurements as a function of temperature show a transition from a ferrimagnetic to a paramagnetic region. The temperature at which this switching takes place is considered as the Curie temperature and is shown in Table II for all the ferrites studied here.

3.3. Microstructural studies by SEM

3.3.1. Particle size distribution of $MgFe_2O_4$

Scanning electron micrographs of all the $MgFe_2O_4$ samples prepared from γ-Fe_2O_3 show a particle size distribution (Fig. 3) up to 3 μm, except for the ferrite MgHEM in which a wide range in sizes up to 6 μm is observed.

MgγFA, MgαFA and MgAmpFA

The sample MgγFA, shows ~ 72% particles between 1–2 μm, 22% grains < 1 μm and 6% in the range of 2–3 μm. The samples MgαFA (γ-Fe_2O_3 source from α-FeOOH) and MgAmpFA (γ-Fe_2O_3 from amp. FeOOH) also show more or less similar grain size distribution to the MgγFA. The micrographs of these are shown in Fig. 4a (MgγFA), Fig. 4b (MgαFA) and Fig. 4c (MgAmpFA). There is a uniform grain size distribution in these samples. The measured porosity from X-ray density and actual density of these are similar: 23.63–26.41 (Table II).

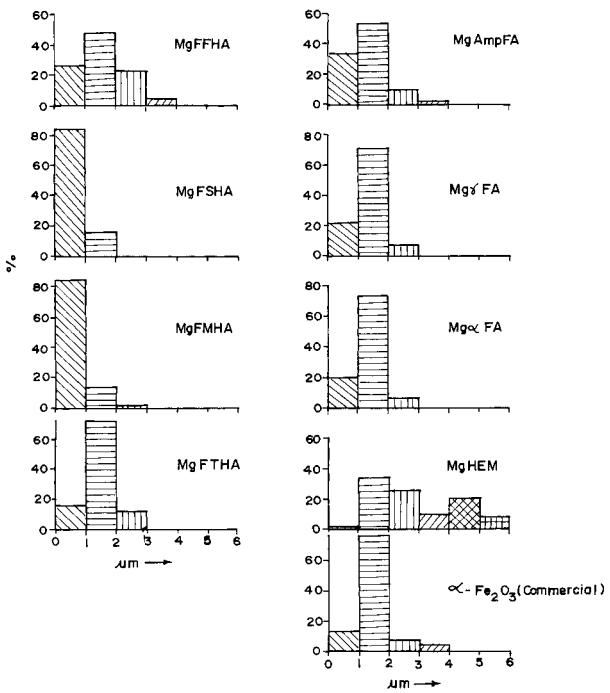

Figure 3 Particle size distribution of $MgFe_2O$ and commercial α-Fe_2O_3.

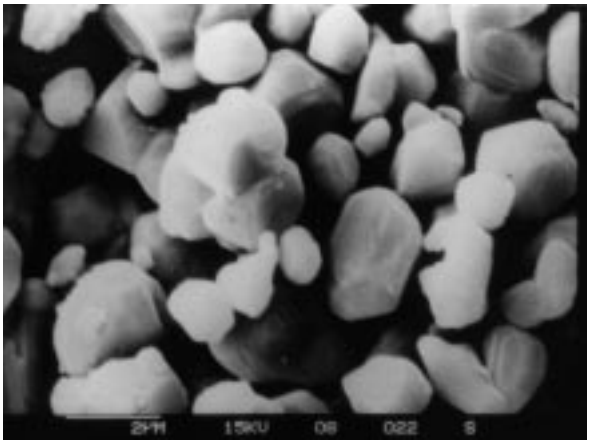

(a)

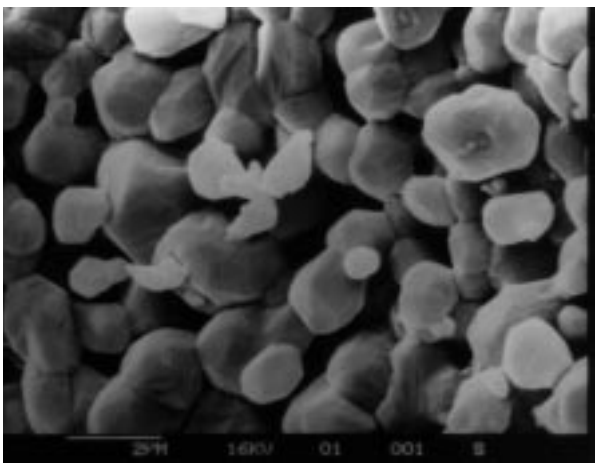

(b)

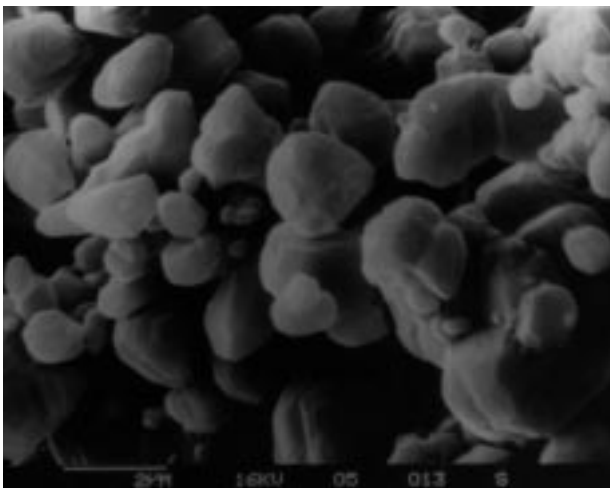

(c)

Figure 4 Scanning electron micrographs of $MgFe_2O_4$: (a) MgγFA, (b) MgαFA and (c) MgAmpFA.

MgFFHA, MgFSHA, MgFMHA and MgFTHA

The $MgFe_2O_4$ synthesized from γ-Fe_2O_3 obtained from iron (II) carboxylato-hydrazinates show a grain distribution of up to 3 μm. The MgFMHA and MgFSHA have $\sim$ 85% grains $<$ 1 μm and $\sim$ 14.4% particles of 1–2 μm. A few particles of 2–3 μm are also observed in MgFMHA. On the other hand, MgFFHA and MgFTHA show a majority of grains sized 1–2 μm. The SEM micrographs are shown in Fig. 5. The porosity of these range from 21–29%.

MgHEM

The $MgFe_2O_4$ prepared from commercial α-Fe_2O_3 shows a wide range of grain size distribution (up to 6 μm). In Fig. 3 it can be seen clearly that 34% of particles are of 1–2 μm, 26% are 2–3 μm, 10% are 3–4 μm, 20% are 4–5 μm and 8% are 5–6 μm in size. Such a distribution of grains effectively makes these samples more porous (SEM micrograph Fig. 6) and the porosity observed from X-ray density and actual density is 42%.

Thus, all samples, except MgHEM, show uniform microstructure. This leads to different magnetic characteristics, as observed in our studies.

3.3.2. Reactivity of iron oxides leading to $MgFe_2O_4$

The $MgFe_2O_4$ synthesized from iron oxide (mainly γ-Fe_2O_3) obtained from different sources show similar micro-structural characteristics with a majority of grains sized $<$ 2 μm. The $MgFe_2O_4$ obtained from commercial α-Fe_2O_3 (MgHEM), however, shows particles up to 6 μm with different grain sizes. The iron oxide (mainly γ-Fe_2O_3) sources used for the synthesis of $MgFe_2O_4$ are from autocatalytically decomposed iron (II) carboxylato-hydrazinates and hydrazinated iron oxyhydroxides. The autocatalytic decomposition leads to oxides of uniform particle size with very high surface area.

The BET surface area of iron oxides (mainly γ-Fe_2O_3) measured by using volumetric adsorption of nitrogen at liquid nitrogen temperature on a few samples are shown to be 30–70 $m^2 g^{-1}$ and SEM micrographs also indicated a uniform distribution of particles of 10–30 nm size. Representative micrographs of FSHA and γFA are shown in Fig. 7a and b, respectively. These iron oxides then react with $MgCO_3$ and the samples sintered at 1000 °C show $<$ 3 μm size grains in the ferrite, as described above.

On the other hand, the wide distribution of particle size in $MgFe_2O_4$ (MgHEM) obtained from commer-

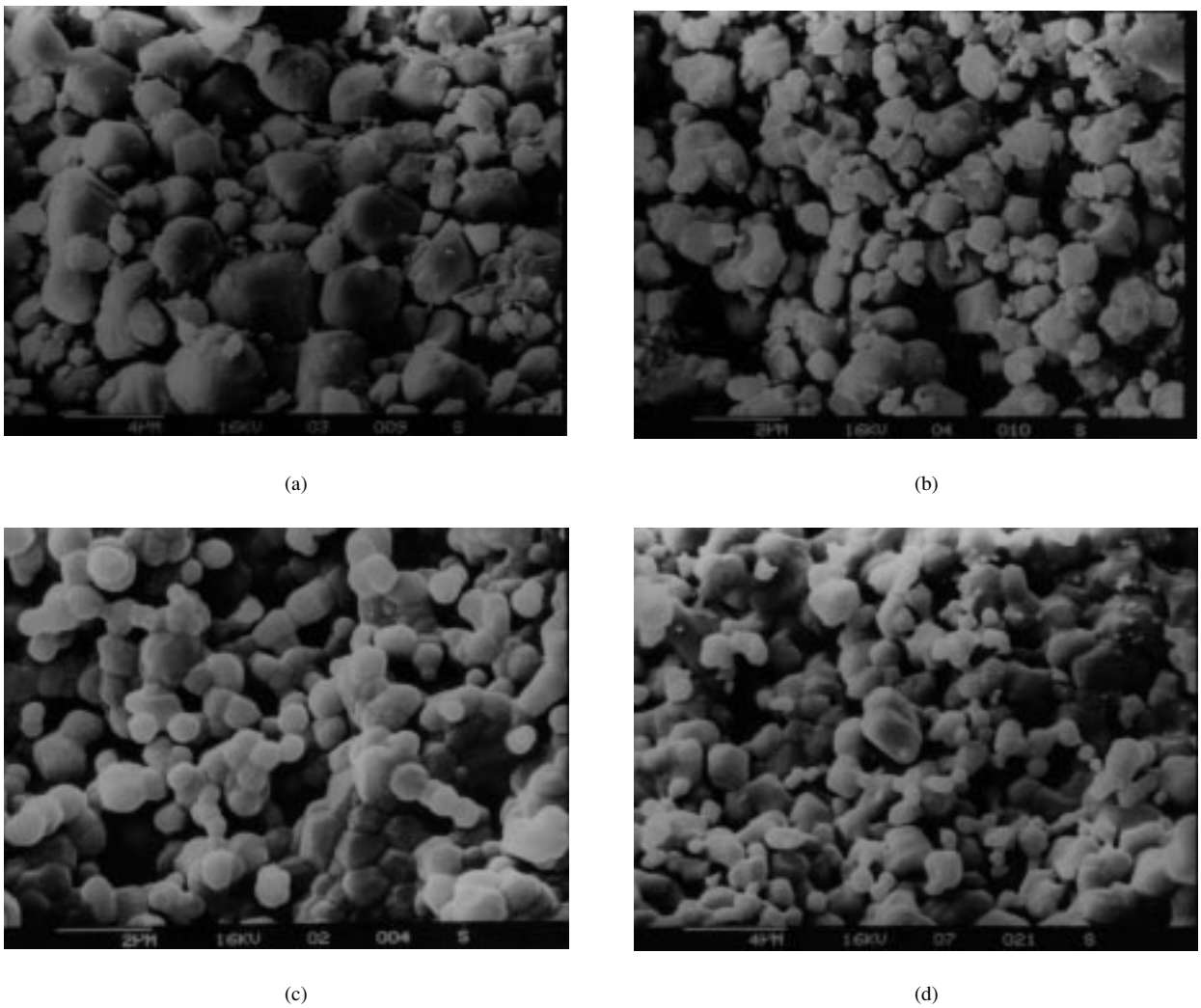

(a) (b) (c) (d)

Figure 5 Scanning electron micrographs of $MgFe_2O_4$: (a) MgFFHA, (b) MgFSHA, (c) MgFMHA and (d) MgFTHA.

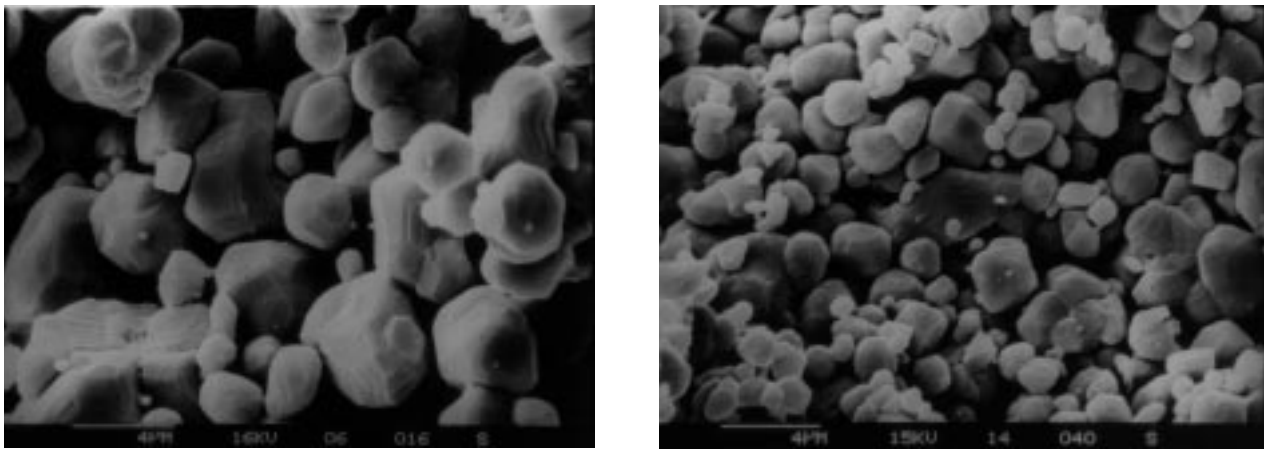

(a) (b)

Figure 6 Scanning electron micrographs of (a) $MgFe_2O_4$: MgHEM (from commercial α-Fe_2O_3) and (b) commercial α-Fe_2O_3

cial α-Fe_2O_3 may be due to the large grain size of 1–2 μm observed in this oxide. In Fig. 3 and Fig. 6b it can be clearly seen that α-Fe_2O_3 (commercial) has 76% of grains 1–2 μm, 13% grains < 1 μm, 7% particles are in the range 2–3 μm, 4% are 3–4 μm. Such a large grain sized α-Fe_2O_3 material compared to small sized γ-Fe_2O_3 is responsible for the wide range of particles in the ferrites with large porosity, as observed in MgHEM (Fig. 6a). The small grain γ-Fe_2O_3 samples, however, give uniform and smaller particles of ferrites with uniform porosity but less than MgHEM. These observations indicate that nanometer size particles give uniform 1–3 μm size ferrites at 1000 °C allowing further scope to increase the particle size by increasing the sintering temperature, giving better characteristics. However, non-uniform particles in MgHEM may further enhance non-uniform grains. Further studies on the influence of sintering temperature on grain size and magnetic characteristics are in progress.

4. Conclusion

1. Iron (II) carboxylato-hydrazinates and iron oxy-hydroxides obtained from iron ore rejects decompose autocatalytically giving mainly γ-Fe_2O_3. A few traces of α-Fe_2O_3 are found in some samples.

2. The iron oxides (mainly γ-Fe_2O_3) yield single phase $MgFe_2O_4$ when mixed with $MgCO_3$ and heated ~ 1000 °C.

3. Commercial α-Fe_2O_3 (hematite) plus $MgCO_3$ at ~ 1000 °C give mainly $MgFe_2O_4$ with a few traces of α-Fe_2O_3, suggesting single phase spinel is not formed.

4. $MgFe_2O_4$ prepared from commercial α-Fe_2O_3 shows high porosity of $\sim 42\%$, while γ-Fe_2O_3 sources result in ferrites of porosity $\sim 25\%$.

5. A low saturation magnetization value of 609 G is observed for $MgFe_2O_4$ prepared from α-Fe_2O_3, whereas the ferrite obtained from all γ-Fe_2O_3 sources show values between 922–1168 G.

6. Curie temperatures T_c of 730, 742 and 739 K are observed for $MgFe_2O_4$ obtained from α-Fe_2O_3 from the

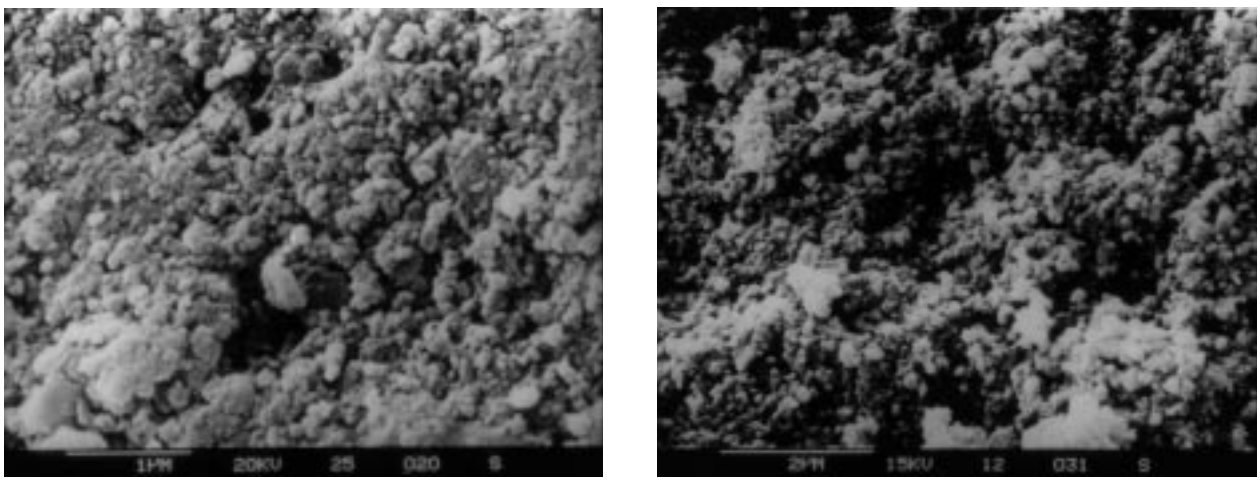

(a) (b)

Figure 7 Scanning electron micrographs of γ-Fe_2O_3 (a) FSHA and (b) γFA.

temperature variation of magnetic susceptibility, initial permeability and resistivity. All other samples showed T_c values lower than this, which are close to the reported values.

7. Uniform grain size in the range of 0–3 μm is observed for $MgFe_2O_4$ from nanometer size γ-Fe_2O_3 prepared from hydrazine precursors. A large distribution in particle size, 0–6 μm, is indicated by $MgFe_2O_4$ synthesized from commercial grade α-Fe_2O_3 of mainly 1–2 μm size grains.

8. The uniform grain size distribution found in $MgFe_2O_4$ obtained from γ-Fe_2O_3 sources give further scope to increase sintering temperature to achieve better magnetic characteristics.

Acknowledgements

KSR wishes to thank the Goa State Council for Science & Technology (GSCS&T), Goa Govt., India for continued financial assistance. The Regional Sophisticated Instrumentation Centre (RSIC), Nagpur, India was prompt in rendering their services for XRD and SEM characterization. The authors are grateful to them. Also, KSR wishes to thank Dr S. R. Sawant, Shivaji University, Kolhapur, India and Dr S. S. Suryavanshi, Centre for Post Graduate Studies of Shivaji University, Solapur for fruitful discussions.

References

1. H. J. HUNH, *Z. Chem.* **27** (1987) 334.
2. J. J. SHROTRI, A. G. BAGUL, S. D. KULKARNI, C. E. DESHPANDE and S. K. DATE, in ''Proc. VI Int Conf. on Ferrites'' (Tokyo, Japan, 1992) p. 404.
3. P. A. TUAN, D. L. MINH, N. CHAU and B. T. CONG, *ibid.*, p. 370.
4. K. J. D. MACKENZIE and C. M. CARDILE, *Thermochim. Acta* **165** (1990) 207.
5. M. L. WANG and Z. W. SHIH, *J. Cryst. Growth* **114** (1991) 435.
6. M. L. WANG and Z. W. SHIH, *ibid.* **116** (1992) 483.
7. K. S. RANE and V. M. S. VERENKAR, *J. Mater. Chem.* (submitted).
8. K. S. RANE and V. M. S. VERENKAR, *ibid.* (submitted).
9. R. G. KULKARNI and H. H. JOSHI, *J. Solid State Chem.* **64** (1986) 141.
10. O. K. SAMUILOVA, V. D. YAGODOVSKII and M. M. KOZLOVA, *Kinet. Catal.* **27** (1986) 208.
11. C. N. RAO and S. R. MURTHY, *Cryst. Res. Technol.* **24** (1989) K6.
12. G. GUSMANO, P. NUNZIANTE, E. TRAVERSA and R. MONTANARY, *Mater. Chem. Phys.* **26** (1990) 513.
13. G. GUSMANO, G. MONTESPERELLI, P. NUNZIANTE and E. TRAVERSA, *J. Mater. Sci.* **28** (1993) 6195.
14. R. GLENN RUPARD and P. K. GALLAGHER, *Thermochim. Acta.* **272** (1996) 11.
15. D. GAJAPATHY and K. C. PATIL, *Mater. Chem. Phys.* **9** (1983) 423.
16. K. C. PATIL, D. GAJAPATHY and V. R. PAI VERNEKAR, *Mater. Res. Bull.* **17** (1982) 29.
17. V. M. S. VERENKAR, PhD Thesis, Goa University, India, 1997 (submitted).
18. JCPDS, Powder diffraction file no. 17–465.
19. S. D. LIKHITE, C. RADHAKRISHNAMURTHY and P. W. SABASRABUDHE, *Rev. Sci. Instrum.* **25** (1965) 302.
20. S. D. LIKHITE and C. RADHAKRISHNAMURTHY, *Curr. Sci.* **35** (1966) 534.
21. JCPDS, Powder diffraction file no. 25–1402.
22. JCPDS, Powder diffraction file no. 24–81.
23. D. KHALAFALLA and A. H. MORRISH, *J. Appl. Phys.* **43** (1972) 624.
24. A. WOLD, *J. Chem. Educ.* **57** (1980) 531.
25. K. SHESHAN, A. L. SHASHIMOHAN, D. K. CHAKRABARTY and A. B. BISWAS, *Phys. Stat. Solidi. A* **68** (1981) 97.
26. G. K. JOSHI, S. A. DESHPANDE, A. Y. KHOT and S. R. SAWANT, *Ind. J. Phys A.* **61** (1987) 251.
27. C. M. SRIVASTAVA, S. N. SHRINGI and M. VIJAYBABU, *Bull. Mater. Sci.* **6** (1984) 27.
28. M. D. SUNDARARAJAN, A. NARAYANASWAMY, T. NAGARAJAN, L. HAGGSTROM, C. S. SWAMY and K. V. RAMANUJACHARY, *J. Phys. C; Solid State Phys.* **17** (1984) 2953.
29. J. SMIT and H. P. J. WIJN, ''Ferrites'' (John Wiley and Sons, New York, 1959) p. 369.
30. S. H. PATIL, S. I. PATIL, S. M. KADAM, S. R. PATIL and B. K. CHOUGULE, *Bull. Mater. Sci.* **14** (1991) 1225.
31. S. A. CHIM, *Ann. Chim. Sci. Mater.* **9** (1974) 31.
32. E. WIESER, H. SCHRODER and K. KLEINCTIJCK, *Phys. Statis A Solid.* **1** (1970) 749.
33. K. SHESHAN, M. J. PATNI and D. K. CHAKRABARTY, *J. Solid State Chem.* **42** (1982) 206.
34. L. M. CORLISS, J. M. HASTINGS and F. G. BROCKMAN, *Phys. Rev.* **90** (1953) 1013.
35. J. S. SMART, *ibid.* **94** (1954) 847.

Received 2 April
and accepted 2 July 1998